

Cinnamaldehyde adsorption and thermal decomposition on copper surfacesa)

Cite as: J. Vac. Sci. Technol. A 39, 053205 (2021); doi: 10.1116/6.0001192 Submitted: 2 June 2021 · Accepted: 16 July 2021 · Published Online: 2 August 2021







Bo Chen, ^{1,b)} Rodrigo Ponce, ² Jonathan Guerrero-Sánchez, ² Noboru Takeuchi, ² and Francisco Zaera ^{1,c)} 10



AFFILIATIONS

- Department of Chemistry and UCR Center for Catalysis, University of California, Riverside, California 92521
- ²Centro de Nanociencias y Nanotecnología, Universidad Nacional Autónoma de México, Apartado Postal 14, Ensenada, Baja California CP 22800, Mexico

Note: This paper is a part of the Special Collection Commemorating the Career of Pat Thiel.

- ^{a)}Contribution for the Special Collection: "Commemorating the Career of Pat Thiel."
- b) Present address: Department of Pathology, Stony Brook University School of Medicine, Stony Brook, NY 11794-8691
- ^{c)}Author to whom correspondence should be addressed: zaera@ucr.edu

ABSTRACT

The uptake and thermal chemistry of cinnamaldehyde on Cu(110) single-crystal surfaces were characterized by temperature-programmed desorption and x-ray photoelectron spectroscopy (XPS). Adsorption at 85 K appears to be initiated by low-temperature decomposition to form styrene, which desorbs at 190 K, followed by the sequential buildup of a molecular monolayer and then a condensed molecular film. Molecular desorption from the monolayer occurs at 410 K, corresponding to a desorption energy of approximately 98 kJ/mol, and further decomposition to produce styrene (again) and other fragmentation products is seen at 550 K. The molecular nature and the quantitation of the low-temperature uptake were corroborated by the XPS data, which also provided hints about the adsorption geometry adopted by the unsaturated aldehyde on the surface. Density functional theory calculations, used to estimate adsorption energies as a function of coverage and coordination mode, pointed to possible η^1 -O binding, at least at high coverages, and to a stabilizing effect on the surface by the aromatic ring of cinnamaldehyde. Finally, coadsorption of oxygen on the surface was found to weaken the binding of cinnamaldehyde to the Cu substrate at high coverages without enhancing its uptake, but to not modify the decomposition mechanism or energetics in any significant way.

Published under an exclusive license by the AVS. https://doi.org/10.1116/6.0001192

I. INTRODUCTION

In catalysis, reactivity and selectivity toward specific pathways are often associated with the adsorption geometry that the reactants adopt on the surface of the catalyst. For instance, in the metalcatalyzed hydrogenation of organic molecules with multiple unsaturated bonds, the double or triple bond that interacts with and binds to the metal is usually the one that incorporates hydrogen atoms first. As a consequence, there is often a tradeoff between total hydrogenation activity, which is high with platinum metals because they bind unsaturated moieties strongly and indiscriminately, and selectivity, which may be controlled by single-coordination adsorption on coinage metals but at the expense of reaction rates.^{2,3} To balance these two trends, there has recently been an interest in combining the two functionalities in a synergistic way. In this single-atom alloy catalysis, a mild metal such as Cu or Au is "spiked"

with a small amount of a more active transition metal (Pt, Pd), presumably to help with the initial activation of H₂ molecules. Although we have recently challenged some aspects of this model,5, it does appear that metals such as Cu may exhibit intrinsic selectivity in hydrogenation reactions, favoring the activation of C=O bonds over C=C moieties during the hydrogenation of unsaturated aldehydes, for instance.

It is, therefore, useful to characterize the adsorption and thermal chemistry of unsaturated aldehydes on metal surfaces using model systems and a modern surface-science approach as a way to better understand and predict adsorption modes for the reactants and selectivities in catalytic hydrogenations and also to help design new, better performing multimetal catalysts. Our past work in this area, using molecular beams, has shown that the hydrogenation of unsaturated aldehydes promoted by Pt surfaces favors the production of saturated aldehydes,8 a result consistent



with what is seen in kinetic experiments with realistic supported catalysts.^{9–11} Infrared absorption spectroscopy experiments^{12–14} and quantum mechanic calculations^{1,4–18} have explained this behavior on the basis of a preference for adsorption with multiple interactions between the unsaturated aldehyde and the metal surface, predominantly via the C=C bond. By contrast, unsaturatedaldehyde hydrogenations on Cu, which needs to be probed with atomic rather than molecular hydrogen in model systems, has shown high intrinsic selectivity toward the production of the unsaturated alcohol, the desired product, via the hydrogenation of the C=O bond. 19 On this metal, recent calculations by us with crotonaldehyde have shown a slight preference for surface bonding in a η^1 configuration through the oxygen atom.^{5,14} Overall, results from the studies with model systems and quantum mechanic calculations available to date suggest that there is a correlation between adsorption mode and catalytic selectivity in these systems. Nevertheless, the pool of compounds probed so far is quite limited, involving mainly acrolein and crotonaldehyde. Here, we expand our previous work to cinnamaldehyde (CMA), with the aim of evaluating the effect of the addition of an aromatic ring to the molecular structure of the reactant. We learned that this results in an additional stabilizing effect via pi-bonding of the ring to the surface but does not change the fundamentals behind the adsorption geometry-reactivity correlation identified before.

II. EXPERIMENT

The experiments were performed in an ultrahigh vacuum (UHV) apparatus equipped with a UTI quadrupole mass spectrometer, used for temperature-programmed desorption (TPD) data acquisition. Up to 15 different masses were monitored in each single TPD run by using a personal computer interfaced to the mass spectrometer. This apparatus was also equipped with x-ray photoelectron spectroscopy (XPS) instrumentation consisting of a 50-mm radius hemispherical electron energy analyzer (VSW HAC 5000) and an aluminum-anode ($hv = 1486.6 \, {\rm eV}$) x-ray source, employed to quantify the CMA uptake and to determine the cleanliness of the surface. Gas dosing was done by backfilling of the chamber using a leak valve and is reported in Langmuirs ($1 \, {\rm L} = 1 \times 10^{-6} \, {\rm Torr} \, {\rm s}$), uncorrected for differences in ion gauge sensitivities. The pressure in the main UHV chamber was measured by using a nude ion gauge.

A Cu single-crystal disk, cut to expose its (110) facet, was polished and mounted on a manipulator capable of $x-y-z-\theta$ motion and of liquid nitrogen cooling and resistive heating, and cleaned *in situ* before each experiment via sputtering-annealing cycles until the surface was deemed clean by XPS and CO TPD. For the experiments on oxidized samples, the surface was then exposed to 50 L of O_2 at 500 K, which was determined to yield a surface coverage of $\theta_O = 0.4$ ML in an incomplete (2×1) structure on the basis of the previous work in our laboratory^{22,23} and the reported literature. CMA (3-phenyl-2-propenal, Sigma-Aldrich, $\geq 95\%$ purity) was placed in a glass container, mounted in a gas manifold, distilled via repeated freeze-pump-thaw cycles, and fed into the UHV chamber as a gas, relying on its high vapor pressure. CMA dosing was carried out at a surface temperature of 85 K, and that temperature ramped in the TPD experiments at a linear rate of 4 K/s.

III. MODELING

Density functional theory (DFT) calculations were performed using the Vienna ab initio Simulation Package (VASP).²⁷ The exchange-correlation energies have been treated according to the Generalized Gradient Approximation (GGA) with Perdew-Burke-Ernzerhof (PBE) parametrization,²⁸ and van der Waals forces have been considered employing the D3 correction method of Grime.²² The one-electron states have been expanded using the projectoraugmented wave (PAW) basis,³⁰ with an energy cutoff of 350 eV. The supercell method has been employed to construct the surface, each supercell composed of a slab formed by four monolayers and a vacuum space of 25 Å. Both (3×3) and (4×4) periodicities in the x-y plane were used, which we associate with high $(\theta_{high} = 1/9 \text{ ML};$ ML = monolayer) and low ($\theta_{low} = 1/16$ ML) coverages, respectively. The Brillouin zone has been sampled with k-point grids of $4 \times 4 \times 1$ and $3 \times 3 \times 1$ for the (3×3) and (4×4) periodicities, respectively, employing the Monkhorst-Pack scheme. The calculated adsorption energies are reported as negative numbers, reflecting the gain in energy upon binding of the molecule to the surface, whereas the energies estimated from TPD results are reported as positive numbers since they refer to the energies required to induce desorption (the reverse of adsorption). It should be noted that the calculations were performed on the (111) surface of copper, not the Cu(110) plane used for the experiments. This is not ideal but was done for simplicity, as the (110) plane offers many more possible adsorption sites. Future calculations will address this difference.

IV. RESULTS

A. Uptake and thermal chemistry of CMA on Cu(110)

The thermal chemistry of CMA was first tested on the Cu (110) surface by TPD. In order to identify the main decomposition products, the signals for multiple amus were recorded in repeated experiments. Representative data for the case of a 5.0 L exposure are shown in Fig. 1. Several distinct peaks are observed. A first sharp desorption feature at 190 K is seen in the 78, 103, and 104 amu traces, which we assign to styrene based on a comparison between the relative intensities measured here and those in the mass-spectra cracking pattern of pure styrene.³¹ Using Redhead's equation³² and a pre-exponential factor of 1×10^{12} s⁻¹ (a typical value used in these calculations), we estimate an activation barrier of $E_{Styrene1,TPD} = 44 \text{ kJ/mol}$ for this reaction. In addition, two features at 245 and 410 K are evident in the traces for 131 and 132 amu (with additional components in the 91, 103, and 104 amu traces) corresponding to molecular CMA; these yield estimated desorption energies of $E_{\text{Multi,TPD}} \sim 57 \text{ kJ/mol}$ and $E_{\text{Mono,}}$ TPD = 98 kJ/mol, respectively, the first quite close to the value reported for CMA sublimation.³³ A fourth peak is seen in the 91 amu trace at approximately 550 K (together with smaller features in the 51, 77, and 104 amu data) that translates into E_{Styrene2}, TPD = 133 kJ/mol, most likely reflecting the desorption of styrene and/or toluene. Finally, signals are seen in the 51, 77, 78, and 103 amu traces over a broad temperature range, roughly between 150 and 400 K, which may be due to other phenyl-containing decomposition products but may originate from reactions on other surfaces (an experimental artifact). Regardless, toluene and other

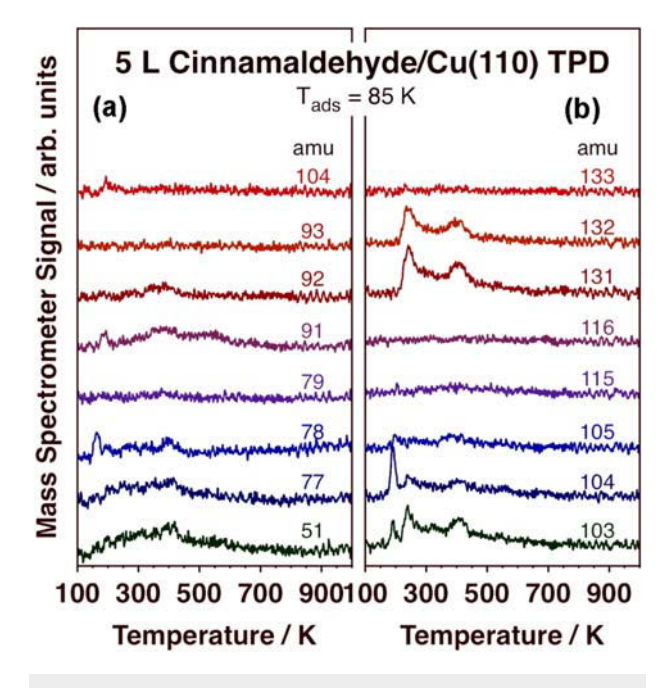
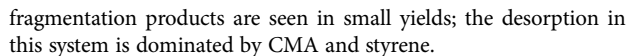


FIG. 1. Representative TPD traces for CMA adsorbed on Cu(110). A $5.0\,L$ exposure was used, and dosing was carried out at $85\,K$. Results from two separate runs are provided focusing on the low (a) and high (b) amu value ranges. The high-amu detection experiment was performed with lower amu resolution to enhance signal sensitivity.



The evolution of the desorption of CMA and styrene was followed as a function of exposure next. The corresponding TPD data are shown in Fig. 2. In terms of molecular desorption, the peak at 410 K is visible even after a 2.0 L exposure and saturates after exposures between 4.0 and 5.0 L, at which point the feature at 245 K starts to grow. We, therefore, assign these two desorption regimes as originating from monolayer and multilayer (condensed) CMA, respectively. Interestingly, the peak associated with styrene at 190 K [Fig. 2(a)] is quite intense even after the 2.0 L exposure and also saturates around 4.0 L, like the CMA monolayer. This fact together with low temperature at which styrene is observed (below the temperature needed to desorb condensed CMA) strongly suggests that some degree of CMA decomposition may take place at very low temperatures, perhaps even during adsorption.

Complementary XPS data were acquired as well. Figure 3 shows the wide-scan traces recorded as a function of CMA exposure at 85 K. Signals for the expected elements, namely, copper, carbon, and oxygen, were all detected, with trends in terms of signal intensity compatible with uptake of the organic molecule on the surface. The peak positions in terms of their binding energies (BEs) are also reflective of this uptake: $BE_{C1s} = 284.7 \text{ eV}$ for the C 1s signal, a value typical of both aliphatic and aromatic hydrocarbons, ³⁴ and $BE_{O1s} = 532.6 \text{ eV}$ for the O 1s peak, as seen for other adsorbed

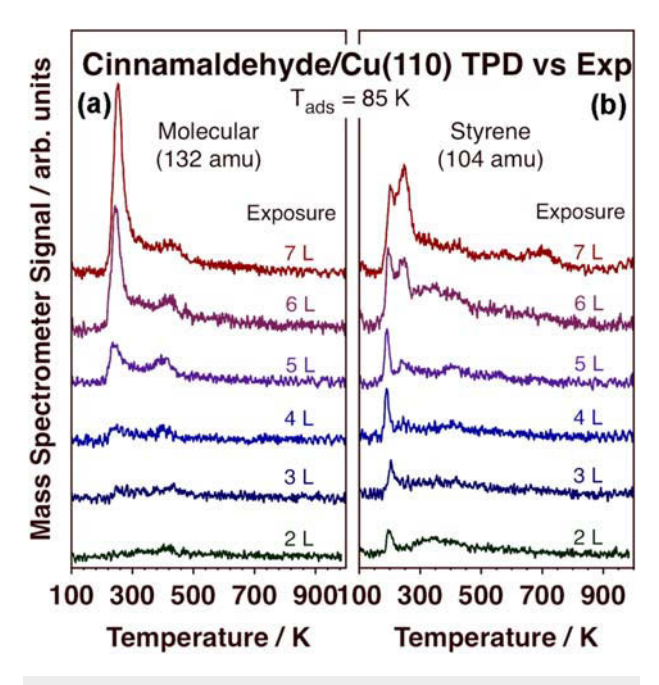


FIG. 2. TPD traces for molecular (132 amu) (a) and styrene (104 amu) (b) desorption from CMA-dosed Cu(110) as a function of exposure.

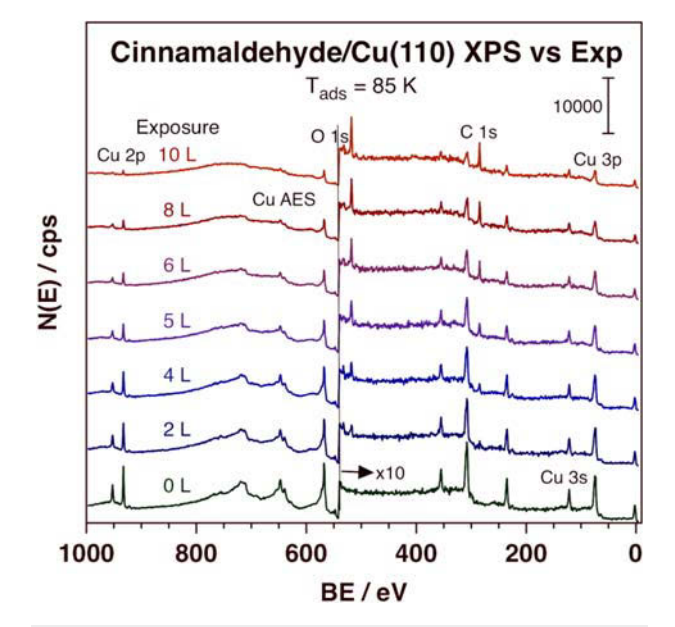


FIG. 3. Wide-scan XPS traces for CMA adsorbed Cu(110) as a function of



unsaturated aldehydes; ³⁵ no appreciable shifts were measured as a function of CMA exposure. The remaining peaks are all associated with metallic copper, the substrate: BE_{Cu3p} = 74.7 eV (Cu 3p), BE_{Cu3s} = 121.6 eV (Cu 3 s), BE_{CuL3VV} = 567.7 eV (Cu L₃VV Auger line; kinetic energy KE_{CuL3VV} = 918.9 eV), BE_{Cu2p3/2} = 932.7 eV (Cu 2p_{3/2}), and BE_{Cu2p1/2} = 952.7 eV (Cu 2p_{1/2}); the resulting value for the Auger parameter (E_{AP} = BE_{Cu2p3/2} + KE_{CuL3VV} = 1851.6 eV) attests to the reduced nature of the metal surface. ³⁴

The TPD and XPS uptake data were quantified in order to determine yields and the monolayer saturation exposure point. The results are presented in Fig. 4. In terms of the TPD data [Fig. 4(a)], saturation of both the CMA monolayer (at 410 K) and the styrene production (190 K) occurs by exposures of between 4 and 5 L (a little earlier in the latter case). Approximately two-thirds of the desorbing molecules at that point are styrene, although this is only a rough estimate as the mass spectrometer signals were not calibrated for individual molecular sensitivities. It is also worth noticing that the yields for CMA lag those for styrene, indicating that perhaps the first adsorbed molecules decompose and produce styrene before reaching the onset of the first desorption peak (~180 K). After exposures beyond 5 L, the only peak that grows is that for CMA at 240 K due to multilayer condensation. It is worth noticing that the leading edge of this peak is identical, within experimental error, in all traces, and that its maximum temperature shifts to higher values with increasing exposure, all signs of the zero-order kinetics expected for desorption from condensed layers.

The XPS uptake data are consistent with the conclusion that monolayer saturation occurs after exposures of about 4-5 L: most

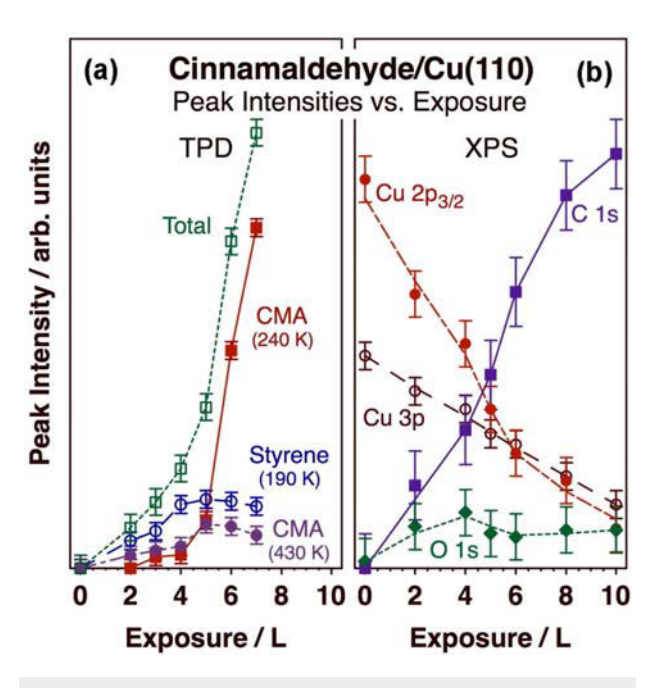


FIG. 4. Quantitation of TPD (a) and XPS (b) peak intensities vs CMA exposure.

traces in Fig. 4(b) show inflection points around that exposure range, indicating a change in the nature of the adsorbed layer. In terms of the Cu data, the inflection is more clearly seen in the Cu 2p_{3/2} peak, as those photoelectrons have low kinetic energy $(KE_{Cu2p3/2} \sim 500 \text{ eV})$ and therefore originate from the few top layers; the Cu 3p photoelectrons, with their higher kinetic energy (KE_{Cu3p} \sim 1400 eV), can come from deeper layers within the bulk and are therefore not as sensitive to changes in the topmost surface layers.³⁷ In addition, the C 1s XPS signal increases with increasing CMA exposure but the slope becomes steeper after monolayer saturation. Interestingly, the O 1s peak stops growing after monolayer saturation, presumably because of a new molecular orientation adopted by the CMA multilayers where the aromatic ring may shield the aldehyde moiety. It should be also indicated that although in Fig. 4 the absolute peak intensities are reported in arbitrary units, the signals were all corrected for their relative sensitivities in the hemispherical analyzer of the XPS instrument.³⁸ Accordingly, it is significant that the signal intensity ratio between the C 1s and O 1s peaks during the buildup of the first monolayer is approximately $C/O_{XPS,1L} = 2.5 \pm 0.5$, much lower that what would be expected based on the stoichiometry of the CMA molecule (C/O = 9). This suggests an adsorption geometry with the oxygen atom exposed and some carbon atoms partially shielded from the outside vacuum, possibly because of the participation of the aromatic ring in the CMA bonding to the surface (perhaps via

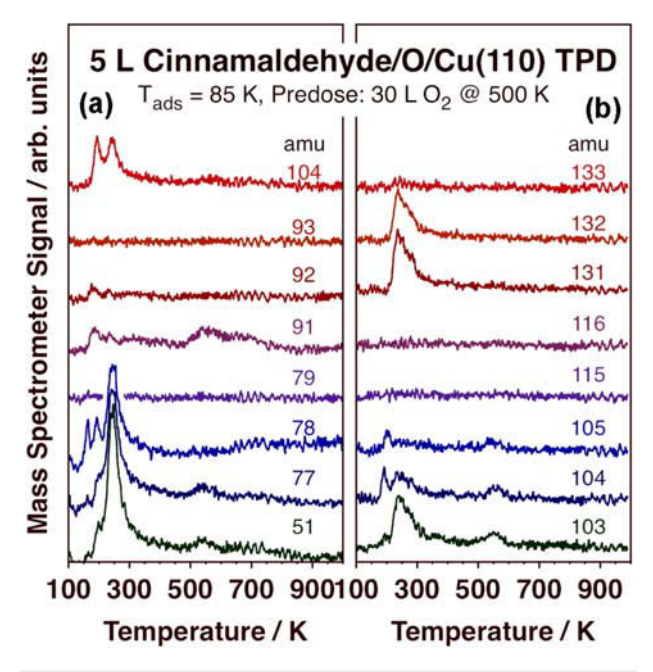


FIG. 5. Representative TPD traces for CMA adsorbed on an oxygen-pretreated (30 L O_2 at 500 K) Cu(110) surface. A 5.0 L exposure was used, and dosing was carried out at 85 K. Results from two separate runs are provided focusing on the low (a) and high (b) amu value ranges. The high-amu detection experiment was performed with lower amu resolution to enhance signal sensitivity.



pi-bonding, in the flat configuration suggested by the DFT data; see below). This $\mathrm{C/O}_{\mathrm{XPS}}$ ratio does grow and approaches the expected stoichiometric value as the condensed layer becomes thicker.

Finally, the adsorption of CMA on an oxygen-pretreated Cu (111) surface was briefly probed by TPD. The motivation for this test was twofold: (1) coadsorbed oxygen has been shown to stabilize the adsorption and increase the uptake of oxygen-containing molecules, including aldehydes^{39,40} and (2) Cu nanoparticles in supported catalysts may be partially oxidized by the trace amounts of O₂ or water often present in reaction mixtures under atmospheric pressures and are likely to be the relevant surface in some hydrogenation catalysis. 41,42 Representative traces from TPD data for 5.0 L of CMA adsorbed on O/Cu(110) at 85 K are shown in Fig. 5. Many similarities can be seen with the case of adsorption on the clean, metallic Cu(110) (Fig. 1), in particular, the fact that peaks are observed for the same amus, indicating the same desorbing products. On the other hand, the yields and the temperatures at which desorption occurs do vary somewhat: styrene (78, 103, 104 amu) still desorbs at 190 K ($E_{O^-Styrene1,TPD} = 44 \text{ kJ/mol}$, multilayer), as in clean Cu(110), but the two peaks for molecular CMA (131, 132 amu) are now seen at 250 K ($E_{O^-Multi,TPD} = 59 \, kJ/mol$, multilayer) and 280 K (E_{O-Mono,TPD} = 66 kJ/mol, monolayer, overlapping the multilayer feature). The first feature coincides, within experimental error, with what was seen in Fig. 1, a result that is expected because this desorption comes from condensed layers and therefore should not be affected by the nature of the surface. CMA

Cinnamaldehyde DFT Structure (3-phenyl-2-propenal)

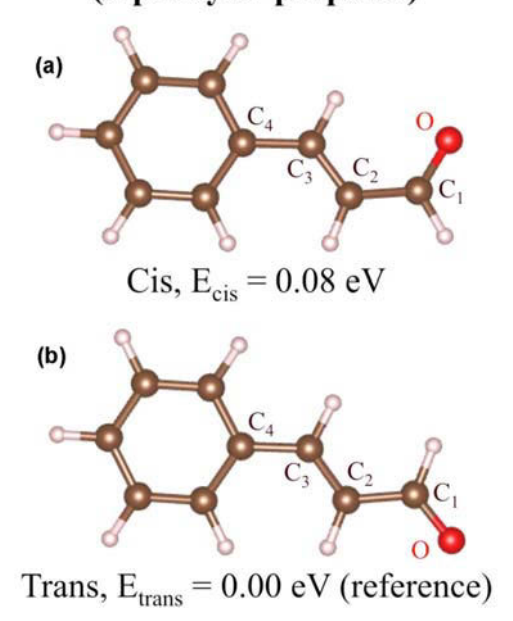


FIG. 6. Optimized structures for isolated *cis* (a) and *trans* (b) CMA molecules, estimated from DFT calculations. Their relative energies are reported as well.

TABLE I. DFT-calculated bond distances for the two isomers of free gas-phase CMA

	Trans	Cis
d(O-C ₁) (Å)	1.26	1.26
$d(C_1-C_2)$ (Å)	1.45	1.46
$d(C_2-C_3)$ (Å)	1.36	1.36
$d(C_3-C_4)$ (Å)	1.46	1.46

desorption from the monolayer, on the other hand, occurs at an $\sim\!130\,\mathrm{K}$ lower temperature, indicating weaker adsorption. The high-temperature product, styrene and/or toluene, seen at 550 K on the clean surface, is more clearly detected in this case (at the same temperature), but there is less desorption of other decomposition products (the 51, 77, 78, and 103 amu traces) in the 150–400 K temperature regime. Lastly, the relative yields of all these compounds in the TPD are also similar in the two cases, on the clean versus oxygen-predosed Cu(110) surfaces. On the whole, there is no evidence to indicate that the preadsorbed oxygen aids in the uptake of CMA on the Cu surface; if anything, it appears to weaken its bonding to the surface.

B. Energetics and structural details of CMA adsorption on Cu(111)

The thermal chemistry of CMA adsorbed on Cu surfaces reported above may be better understood on the basis of the way the molecule bonds to the surface. To that effect, we have carried out

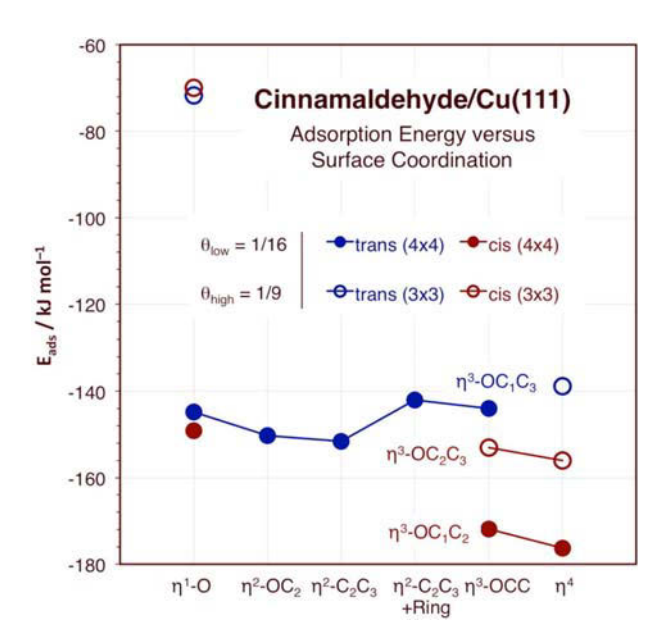


FIG. 7. Adsorption energies, from DFT calculations, for CMA as a function of surface coordination. Data are provided for both *cis* and *trans* isomers and for two surface coverages.



complementary DFT calculations. For reference, the structure and energetics of the gas-phase CMA were determined first. There are two isomers (*cis* and *trans*, or E and Z) of this molecule, but the *trans* configuration is the most stable and the main component of the commercial liquid (according to the 1H NMR data provided by the manufacturer); our calculations estimate the energy difference between the two to be approximately $\Delta E_{\text{cis-trans.gas}} \sim 0.08 \, \text{eV} = 7.7 \, \text{kJ/mol}$ (Fig. 6), the same as for crotonaldehyde, yielding an equilibrium composition with about 95% *trans*-CMA at room temperature. 43 The calculated structural parameters of both isomers are reported in Table I. The shorter O=C₁ and C₂=C₃ bonds are a clear indication of their double-bond character.

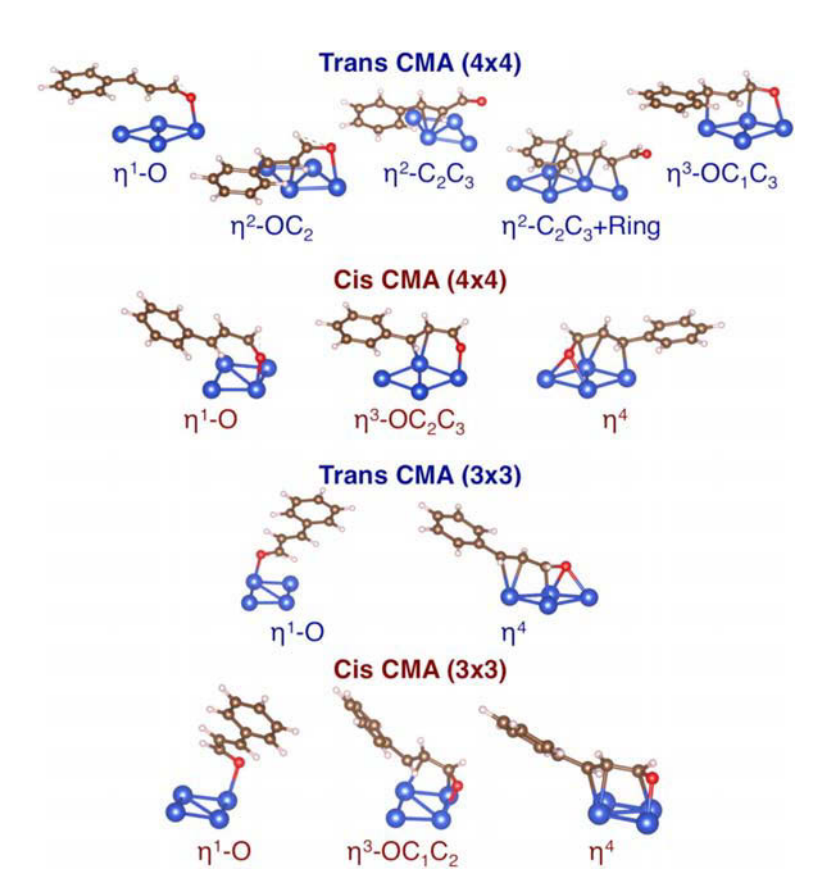
CMA adsorption on Cu(111) was calculated next. As indicated in Sec. III, two different unit cells with (4 × 4) and (3 × 3) periodicity were used to emulate low ($\theta_{low} = 1/16 \text{ ML}$) and high ($\theta_{high} = 1/9 \text{ ML}$) coverages, respectively. The adsorption energy E_{ads} was calculated as

$$E_{ads} = E_{CMA@surface} - E_{surface} - E_{CMA}$$
,

where $E_{CMA@surface}$ and $E_{surface}$ are the total energies of the slab with and without the cinnamaldehyde molecule, and E_{CMA} is the total energy of cinnamaldehyde in the trans configuration in the gas phase. It is important to keep in mind that in this report more negative adsorption energy values correspond to more stable configurations.

The energetics and the atomic structures obtained from our DFT calculations are summarized in Figs. 7 and 8, respectively. Figure 7 shows that for both low and higher coverages adsorption of the cis isomer is more stable than adsorption of the trans isomer. Nevertheless, the original molecule is mainly in its trans configuration (as mentioned above) and that is the isomer expected to be seen on the surface. It is also significant that the adsorption energy at low coverages does not vary much regardless of the coordination mode of the molecule to the surface. This is best illustrated by the case of trans-CMA adsorbed on the (4×4) cell, where the adsorption energy varies only between $E_{trans-low,DFT} = -140$ and $-150 \, kJ/mol$ when going from single coordination through the oxygen atom $(\eta^1$ -O) to bonding via three atoms $(\eta^3$ -OC₁C₃). Only when the coverage that is high, that is, when a small unit cell is used in the calculations, strong steric effects and intermolecular interactions cause some coordinations to become less stable. It is curious that it is the η^{1} -O bonding mode the one that seems to show the largest destabilization effect, as the adsorption energies in those cases are reduced to values of about $E_{high,DFT} \sim -70$ kJ/mol for both isomers. All this is to be contrasted with our experimental TPD results, which yielded a desorption energy for the monolayer of $E_{\text{Mono,TPD}} = 98 \text{ kJ/mol}$, somewhere in between the values estimated by DFT.

Another important observation from the DFT results is that the adsorption of cinnamaldehyde on Cu(111) is much stronger



 $\begin{tabular}{ll} FIG. & 8. & Optimized structures for the CMA adsorption coordinations reported in Fig. 7. \\ \end{tabular}$



TABLE II. Structural parameters for the optimized configurations of cinnamaldehyde on Cu(111) at low coverage ($\theta = 1/16$ ML).

	Trans-CMA					Cis-CMA		
(4×4) Unit cell	η^1 -O	η^2 -OC ₂	η^2 - C_2C_3	η^2 -C ₂ C ₃ +ring	η^3 -OC ₁ C ₃	η^1 -O	η^3 -OC ₂ C ₃	η^4
d(O-C ₁) (Å)	1.30	1.33	1.27	1.26	1.35	1.32	1.33	1.37
$d(C_1 - C_2)$ (Å)	1.43	1.43	1.45	1.45	1.42	1.42	1.42	1.41
$d(C_2 - C_3)$ (Å)	1.38	1.41	1.41	1.43	1.43	1.39	1.42	1.44
$d(C_3 - C_4)$ (Å)	1.44	1.44	1.44	1.43	1.46	1.45	1.46	1.45
d(O-Cu) (Å)	2.13	2.11	_	_	_	2.02	2.03	2.14
$d(C_1-Cu)$ (Å)	_	_	_	_	2.17	_	_	2.22
$d(C_2-Cu)$ (Å)	_	2.32	2.40	2.21	_	_	2.39	2.45
$d(C_3$ — $Cu)$ (Å)	_	_	2.27	2.32	2.22	_	2.23	2.19

than that of other unsaturated aldehydes: the range of adsorption energies reported here ($E_{ads,CMA} \sim -140$ to -150 kJ/mol, except for the singly coordinated adsorption at high coverages) is at least 50 kJ/mol higher in absolute terms than our reported values for crotonaldehyde $(E_{ads,CRO} \sim -75 \, kJ/mol)^{14}$ and our tentative estimate for acrolein ($E_{ads,ACR} \sim -90 \text{ kJ/mol}$). One possible explanation for this discrepancy may be that in the case of CMA there is an additional interaction between the aromatic ring and the surface, perhaps via pi-bonding. In support of this hypothesis, we point to the observation that in most of the optimized geometries for adsorbed CMA reported in Fig. 8 the phenyl ring is close to the Cu surface and oriented with its plane parallel or at most slightly tilted with respect to that of the exposed metal plane. Moreover, the energies for benzene and styrene adsorbed on Cu(111) in a flat geometry were estimated [using the large (4×4) unit cell] to be $E_{ads,Benz} = -96.9 \text{ kJ/mol}$ and $E_{ads,Styr} = -130.9 \text{ kJ/mol}$, respectively, values comparable to the $\Delta E = E_{ads,CMA} - E_{ads,CRO}$ difference discussed here. A flat aromatic ring adsorption was also inferred from the XPS data, as discussed above in reference to the data in Fig. 4. It should be kept in mind that such configurations may not be stable at high coverages because of steric effects, and that more tilted arrangements may be the norm then. A transition between flat-lying and tilted aromatic rings on surfaces is common and has been reported repeatedly in the past. 36,44-47 However, at the high-

TABLE III. Structural parameters for the optimized configurations of cinnamaldehyde on Cu(111) at high coverage ($\theta = 1/9$ ML).

	Trans-CMA		Cis-CMA				
(3×3) Unit cell	η ¹ -Ο	η^4	η ¹ -Ο	η^3 -OC ₁ C ₂	η^4	$\eta^{4^{'}}$	
d(O-C ₁) (Å)	1.28	1.35	1.30	1.33	1.33	1.34	
$d(C_1-C_2)$ (Å)	1.42	1.44	1.42	1.43	1.44	1.43	
$d(C_2-C_3)$ (Å)	1.37	1.40	1.37	1.42	1.41	1.41	
$d(C_3-C_4)$ (Å)	1.45	1.46	1.44	1.46	1.46	1.46	
d(O-Cu) (Å)	2.07	2.13, 2.19	2.05	2.00	2.01	2.02	
$d(C_1-Cu)$ (Å)	_	2.18	_	_	2.30	2.19	
$d(C_2-Cu)$ (Å)	_	2.25	_	2.17	2.20	2.23	
$d(C_3-Cu)$ (Å)	_	2.45	_	_	2.50	2.41	

coverage end, the energy loss from tilting the rings away from the surface may be compensated, at least in part, by pi-pi intermolecular interactions that require proximity possibly not available in the CMA case; the end result is that $\eta^1\text{-O}$ adsorption appears viable for $\theta=1/9$ ML but with a much lower absolute adsorption energy $(E_{\rm high0,DFT}\sim-70~kJ/mol)$ than what is estimated at $\theta=1/16$ ML.

Finally, the structural parameters of CMA adsorbed on Cu (111) in the different configurations identified in this study are summarized in Tables II and III. At low coverages ($\theta = 1/16 \text{ ML}$, Table II), the changes in bond lengths seen upon adsorption are very similar for the two (cis and trans) isomers. Specifically, an increase in the $O=C_1$ and $C_2=C_3$ bond lengths is seen in all cases, indicating the rehybridization of these double bonds upon adsorption. For instance, $d(O-C_1) = 1.30-1.33$ Å for the η^1 -O and η^2 -OC₂ configurations of both isomers, a distance much larger than the $d(O-C_1)_{gas} = 1.26 \text{ Å}$ value seen in the free CMA molecule (Table I), and similarly, $d(C_2-C_3) \sim 1.4$ Å for those adsorbates, somewhere in between what is expected for single and double bonds. As expected, less rehybridization of the carbonyl group is seen in the η^2 -C₂C₃ adsorption configurations, because in those cases the C=O moiety does not significantly interact with the surface; the same can be said for the C=C bond in the η^1 -O adsorption mode. At the other extreme, all bond distances in the cis η⁴ configuration have large values typical of single character, even though the C₃—Cu distance is quite long, indicating a weak interaction. The distances of the C₁-C₂ and C₃-C₄ bonds are not altered nearly as much and retain much of the single character seen with the isolated molecule.

At higher coverages ($\theta = 1/9$ ML, Table III), only a few configurations are stable, and, for both the *cis* and *trans* isomers, the most stable configuration is with multiple coordinations, η^4 . It appears that this coverage is still low enough to allow for full interaction between the adsorbate and the surface. Also, the structural parameters in this case do not change much compared with those seen at the lower coverage.

V. DISCUSSION AND CONCLUSIONS

As stated in Sec. I, the aim of this work was to develop an understanding of the adsorption and surface chemistry of cinnamaldehyde on copper surfaces in order to contrast them with the behavior of other unsaturated aldehydes (acrolein, crotonaldehyde)



and to correlate with reported catalytic behavior. It was determined, on the basis of results from TPD experiments, that adsorption of CMA on Cu(110) leads to partial decomposition even at cryogenic temperatures, as a desorption peak for styrene is seen at 190 K. On the other hand, the remainder of the molecular adsorbates binds fairly strongly to the Cu surface, $E_{Mono,TPD} = 98 \text{ kJ/mol.}$ Even higher monolayer binding energies were estimated by DFT $(E_{low\theta,DFT} = -140 \text{ to } -150 \text{ kJ/mol})$, but the discrepancy may be attributed to coverage effects; adsorption at higher coverages can be as weak as $E_{high\theta,DFT} = -70 \text{ kJ/mol}$. These energies do not vary much with coordination structure at low coverages, as similar values were calculated for the whole range between η¹ and η⁴ bonding, but more discrimination and preference for less coordination (η^1 -O), even if at lower energies, may be seen at high coverages. A second styrene desorption peak was also observed in the TPD traces at 550 K, corresponding to $E_{Styrene2,TPD} = 133 \text{ kJ/mol.}$

This dynamics between surface coverage and adsorption energy may play a critical role in the TPD results as well as in the catalytic observations reported by others in the past. In TPD, coverages vary as desorption takes place, so the initial high coverages may lead to weak adsorption, which in turn facilitates partial desorption. Once the low-temperature desorption peaks reach a determined yield, however, the surface coverage of the remaining adsorbates is reduced and the adsorption geometry changes to multiple coordination, increasing the adsorption energy. This is typical with aromatic compounds and justifies the detection of the hightemperature desorption peaks for CMA and styrene seen in the TPD results. Critically, a different dynamics takes place under catalytic conditions, where the adsorbate may reach a high steady-state coverage and therefore does not experience the high-temperature TPD behavior described above. Therefore, a η^1 -O coordination may be the relevant intermediate during catalytic hydrogenations, accounting for the observed selectivity toward the unsaturated alcohol.

Two more observations derive from this work that are worth mentioning. The first is the fact that CMA appears to bind to Cu much more strongly than either acrolein or crotonaldehyde. This was accounted for here by the extra pi interaction of the aromatic ring in CMA with the surface. The difference is clearly relevant to the adsorption behavior seen in the model single-crystal surfaces, but may not be as important during catalysis, again because of the higher coverages involved under those conditions. On the other hand, additional intermolecular pi-pi stabilizing interactions not seen in UHV may participate. This would need to be explored further.

Lastly, the effect of coadsorbed oxygen was briefly tested. The stabilizing effect seen with alcohols and expected for aldehydes was not seen here, however. Indeed, no significant increase in CMA uptake by the surface was detected upon predosing oxygen atoms, and a significant weakening of the monolayer molecular adsorption was measured instead, with the TPD desorption energy decreasing from $E_{\rm Mono,TPD}=98~kJ/mol$ to $E_{\rm O^-Mono,TPD}=66~kJ/mol$. Styrene production was still seen at the same high temperature (550 K) as on the clean Cu, however, indicating that adsorption at low coverages may not change much upon oxygen coadsorption. It would appear that surface coverage rather than oxidation state defines the surface chemistry in these systems.

ACKNOWLEDGMENTS

Financial support for this project was provided by a grant from the U.S. National Science Foundation, Division of Chemistry (Grant No. NSF-CHE1953843). N.T., R.P., and J.G.-S. thank DGAPA-UNAM (Project Nos. IN101019 and IA100920) and Conacyt (Grant No. A1-S-9070) for partial financial support. Calculations were performed in the DGCTIC-UNAM Supercomputing Center (Project Nos. LANCAD-UNAM-DGTIC-051 and LANCAD-UNAM-DGTIC-368).

DATA AVAILABILITY

The data that support the findings of this study are available from the corresponding author upon reasonable request.

REFERENCES

- ¹F. Zaera, ACS Catal. 7, 4947 (2017).
- ²L. Zhang, M. Zhou, A. Wang, and T. Zhang, Chem. Rev. 120, 683 (2020).
- ³M. Luneau, J. S. Lim, D. A. Patel, E. C. H. Sykes, C. M. Friend, and P. Sautet, Chem. Rev. 120, 12834 (2020).
- ⁴R. T. Hannagan, G. Giannakakis, M. Flytzani-Stephanopoulos, and E. C. H. Sykes, Chem. Rev. 120, 12044 (2020).
- ⁵Y. Cao, B. Chen, J. Guerrero-Sánchez, I. Lee, X. Zhou, N. Takeuchi, and F. Zaera. ACS Catal. 9, 9150 (2019).
- ⁶Y. Cao, J. Guerrero-Sańchez, I. Lee, X. Zhou, N. Takeuchi, and F. Zaera, ACS Catal. 10, 3431 (2020).
- ⁷X. Lan and T. Wang, ACS Catal. 10, 2764 (2020).
- ⁸Y. Dong and F. Zaera, J. Phys. Chem. Lett. 9, 1301 (2018).
- ⁹P. Gallezot and D. Richard, Catal. Rev. Sci. Technol. 40, 81 (1998).
- ¹⁰Y. Yuan, S. Yao, M. Wang, S. Lou, and N. Yan, Curr. Org. Chem. 17, 400 (2013).
- ¹¹L. J. Durndell, K. Wilson, and A. F. Lee, RSC Adv. 5, 80022 (2015).
- ¹²J. C. de Jesús and F. Zaera, J. Mol. Catal. A Chem. **138**, 237 (1999).
- ¹³J. C. de Jesús and F. Zaera, Surf. Sci. **430**, 99 (1999).
- ¹⁴M. T. Nayakasinghe, J. Guerrero-Sánchez, N. Takeuchi, and F. Zaera, J. Chem. Phys. 154, 104701 (2021).
- ¹⁵F. Delbecq and P. Sautet, J. Catal. 211, 398 (2002).
- ¹⁶D. Loffreda, F. Delbecq, F. Vigne, and P. Sautet, Angew. Chem., Int. Ed. 44, 5279 (2005).
- ¹⁷D. Loffreda, F. Delbecq, F. Vigne, and P. Sautet, J. Am. Chem. Soc. **128**, 1316 (2006).
- ¹⁸J. Haubrich, D. Loffreda, F. Delbecq, P. Sautet, Y. Jugnet, C. Becker, and K. Wandelt, J. Phys. Chem. C 114, 1073 (2010).
- ¹⁹B. Chen and F. Zaera, J. Phys. Chem. C 125, 14709 (2021).
- ²⁰T. Kim and F. Zaera, J. Phys. Chem. C 116, 8594 (2012).
- ²¹Y. Yao, J. Guerrero-Sánchez, N. Takeuchi, and F. Zaera, J. Phys. Chem. C 123, 7584 (2019).
- ²²Y. Yao and F. Zaera, Surf. Sci. 650, 263 (2016).
- ²³Y. Yao and F. Zaera, Surf. Sci. **646**, 37 (2016).
- ²⁴A. G. J. De Wit, R. P. N. Bronckers, and J. M. Fluit, Surf. Sci. 82, 177 (1979).
- 25 F. M. Chua, Y. Kuk, and P. J. Silverman, Phys. Rev. Lett. 63, 386 (1989).
- ²⁶R. Feidenhans'l, F. Grey, R. L. Johnson, S. G. J. Mochrie, J. Bohr, and M. Nielsen, Phys. Rev. B 41, 5420 (1990).
- ²⁷G. Kresse and J. Furthmüller, Phys. Rev. B **54**, 11169 (1996).
- ²⁸J. P. Perdew, K. Burke, and M. Ernzerhof, Phys. Rev. Lett. 77, 3865 (1996).
- ²⁹S. Grimme, J. Antony, S. Ehrlich, and H. Krieg, J. Chem. Phys. **132**, 154104 (2010).
- **30**P. E. Blöchl, Phys. Rev. B **50**, 17953 (1994).
- ³¹S. E. Stein, "NIST mass spec data center," in NIST Chemistry WebBook: NIST Standard Reference Database Number 69, edited by P. J. Linstrom and



- W. G. Mallard (National Institute of Standards and Technology, Gaithersburg, MD, 2018), accessed June 10, 2021.
- 32P. A. Redhead, Vacuum 12, 203 (1962).
- 33See http://webbook.nist.gov/chemistry/ for NIST Standard Reference Database
- (2003). ³⁴Handbook of X-Ray Photoelectron Spectroscopy, edited by C. D. Wagner, W. M. Riggs, L. E. Davis, J. F. Moulder, and G. E. Muilenberg (Perkin-Elmer Corporation, Eden Prairie, MN, 1978).

 35 F. Bournel, C. Laffon, P. Parent, and G. Tourillon, Surf. Sci. 350, 60 (1996).
- 36 F. Zaera, in Comprehensive Inorganic Chemistry II, edited by J. Reedijk and K. Poeppelmeier (Elsevier, Oxford, 2013), pp. 39–74.

 37
 M. P. Seah and W. A. Dench, Surf. Interface Anal. 1, 2 (1979).
- ³⁸Practical Surface Analysis. Volume 1. Auger and X-ray Photoelectron Spectroscopy, edited by D. Briggs and M. P. Seah (John Wiley and Sons, Chichester, 1990).

- 39 J. P. Camplin and E. M. McCash, Surf. Sci. 360, 229 (1996).
- 40 W. Li, G. Fan, L. Yang, and F. Li, Catal. Sci. Technol. 6, 2337 (2016).
- ⁴¹F. Xu, K. Mudiyanselage, A. E. Baber, M. Soldemo, J. Weissenrieder, M. G. White, and D. J. Stacchiola, J. Phys. Chem. C 118, 15902 (2014).
- 42 M. B. Gawande, A. Goswami, F.-X. Felpin, T. Asefa, X. Huang, R. Silva, X. Zou, R. Zboril, and R. S. Varma, Chem. Rev. 116, 3722 (2016).
- 43 Y.-J. Yang, B.-T. Teng, Y. Liu, and X.-D. Wen, Appl. Surf. Sci. 357, 369
- (2015). 44H. Hoffmann, F. Zaera, R. M. Ormerod, R. M. Lambert, L. P. Wang, and W. T. Tysoe, Surf. Sci. 232, 259 (1990).
- ⁴⁵F. P. Netzer and M. G. Ramsey, Crit. Rev. Solid State Mater. Sci. 17, 397
- ⁴⁶J. Kubota and F. Zaera, J. Am. Chem. Soc. **123**, 11115 (2001).
- 47G. Canduela-Rodriguez, M. K. Sabbe, M.-F. Reyniers, J.-F. Joly, and G. B. Marin, Phys. Chem. Chem. Phys. 16, 23754 (2014).